OPTIMAL RECONFIGURATIONS OF TWO-CRAFT COULOMB FORMATION IN CIRCULAR ORBITS

Ravi Inampudi and Hanspeter Schaub

Simulated Reprint from

Journal of Guidance, Navigation and Control

Volume 35, Number 6, November–December 2012, Pages 1805–1815

A publication of the
American Institute of Aeronautics and Astronautics, Inc.
1801 Alexander Bell Drive, Suite 500
Reston, VA 22091

Optimal Reconfigurations of Two-Craft Coulomb Formation in Circular Orbits

Ravi Inampudi* and Hanspeter Schaub†

Optimal reconfigurations of a two-spacecraft Coulomb formation are determined by applying nonlinear optimal control techniques. The objective of these reconfigurations is to maneuver the two-craft formation between two charged equilibria configurations. The four optimality criteria considered are minimum time, minimum acceleration of the separation distance, minimum electric propulsion fuel usage, and minimum electrical power consumption. The reconfiguration between equilibra is first considered by varying the desired separation distance. In a radial relative equilibrium configuration, only the Coulomb force is required to control the in-plane motion and to steer the satellites from their initial to their final radial position. In this reconfiguration maneuver, the gravity gradient torque is exploited to stabilize the in-plane motion. For along-track and orbit normal equilibrium locations, the reconfiguration maneuver requires hybrid controls. Here the Coulomb force is varied to control the separation distance and inertial micro-thrusters are activated for control in the transverse directions. Second, a reconfiguration involving hybrid control is used to maneuver the crafts from any initial equilibrium position to a final one. The goal is to determine optimal maneuvers maximizing the use of Coulomb propulsion while minimizing the electric propulsion usage. The two-point boundary value problem optimization formulation is numerically solved via pseudo-spectral methods. Pontryagin's Minimum Principle verifies the open loop solutions' optimality.

I. Introduction

The concept of using Electrostatic propulsion to control satellite formations with separation distances on the order of dozens of meters is introduced in References 1 and 2. Active spacecraft charge transfer generates inter-spacecraft Coulomb forces to control the spacecraft formation shape and size. At small separation distances between spacecraft, such propellant-less thrusting is an attractive solution over conventional electric propulsion to avoid thruster plume contamination of the neighbouring spacecraft. Furthermore, Coulomb propulsion is a highly efficient system with a renewable energy source, I_{sp} values ranging up to 10^{13} seconds, and it has very little electrical power requirements (one Watt or less). These advantages enable high precision, close-proximity formation flying with several potential applications in space technologies; for example, high accuracy wide-field-of-view optical interferometry missions, spacecraft cluster control, as well as rendezvous and docking maneuvers. Despite these advantages, Coulomb propulsion has a few

*Graduate Student, Aerospace Engineering Sciences Department, University of Colorado, Boulder, CO. AIAA Member

†Associate Professor, H. Joseph Smead Fellow, Aerospace Engineering Sciences Department, University of Colorado, Boulder, CO. AIAA Associate Fellow

drawbacks. The formation dynamics are highly coupled and nonlinear; dependence of the inter-spacecraft Coulomb forces of the whole formation on each and every spacecraft's position and charge; and feasibility of Coulomb formation flying concept in less dense plasma environments at geostationery orbit (GEO) altitudes or higher. Moreover, as the electrostatic forces are internal to the formation, Coulomb forces cannot be used to reorient a full formation to a new orientation. Therefore, to reorient a Coulomb formation, external forces such as thrusters or differential gravity gradient torques must be used.

Parker and King[1,2] present analytic open-loop solutions for Hill-frame invariant static Coulomb formations with symmetry assumptions. The charges required to maintain the formation shape are held constant and the spacecraft are placed at pre-defined locations in the rotating Hill frame. Consequently, the Coulomb forces perfectly cancel all relative motion of the charged spacecraft, causing the static Coulomb formation to appear fixed as seen in the Hill frame. References 3–5 present systematic analytic solutions for two, three, and four-spacecraft formations. Furthermore, Berryman and Schaub[5] numerically demonstrate that charged equilibria with as many as nine craft are possible in GEO orbits. The open-loop static Coulomb formations are all dynamically unstable without a feedback control law to stabilize the motion. Reference 6 develops a charge control law to reposition a charged body using three charged drones. The control law neglects the orbital mechanics and considers only Coulomb attraction as the dominant force acting on a system. Reference 7 explores a different Coulomb force deployment technique in which a chief satellite repositions small deputy spacecraft from an initial configuration near the chief to a specified shape outward from the chief. References 8 and 9 propose a distributed navigation technique called Equilibrium Shaping (ES) to drive a swarm of satellites to a desired configuration in space. This method exploits a decentralized path-planning algorithm requiring a small amount of communication between the satellites and gives each satellite the autonomous ability to decide a position in the target formation. The method is demonstrated though numerical simulations and suitable for very large swarms of spacecraft; however, each spacecraft pursues suboptimal maneuvers due to the highly decentralized scheme, and the control algorithm does not have analytical stability guarantees.

Stabilization techniques of two-craft virtual Coulomb structure in equilibrium configurations (radial, along-track, and orbit normal) are studied in Reference 10. About an orbit radial direction, to stabilize the relative separation distance a charge feedback law is used exploiting the differential gravitational attraction to stabilize the in-plane attitude. Along the orbit-normal and the along-track directions, the charge feedback law and the differential gravitational accelerations are inadequate to stabilize the in-plane motion. Therefore, for asymptotic in-plane stabilization, hybrid feedback control laws are used which combine conventional thrusters and Coulomb forces. Furthermore, Reference 10 investigates the linear dynamics and stability analysis of reconfiguration maneuvers for all three equilibrium configurations using linearized time-varying dynamical models. In such reconfiguration maneuvers as shown in Figure 1(a), varying electrostatic Coulomb forces can increase or decrease the relative distance between the two satellites. These Coulomb tether expansion and contraction rates affect the stability of the virtual structure within particular limits, and the reconfigurations thus obtained are suboptimal. Moreover, such linearized models could not be used in the nonlinear regime to perform reconfigurations such as a radial to along-track reconfiguration shown in Figure 1(b). Therefore, optimal control techniques could provide an alternative direction to determine optimized reconfiguration maneuvers for constrained nonlinear systems.

Optimal control problems concerning deployment/retrieval of a tethered subsatellite using various performance metrics are considered in References 11, 12 and 13. However, such solutions are not unique and depend on the performance index chosen to solve the optimal control problem. Reference 13 provides a comprehensive study of the effect of different performance indices on the optimal deployment and retrieval dynamics. For example, for a rigid tether, minimizing the length acceleration or minimizing functions of the tension acceleration appear to give good trajectories in terms of the maximum variations in the states and accelerations. Furthermore, optimal design problems in space applications almost always imply minimizing fuel use, which dictates the engineering feasibility of any mission.[14] Also, Reference 14 discusses how

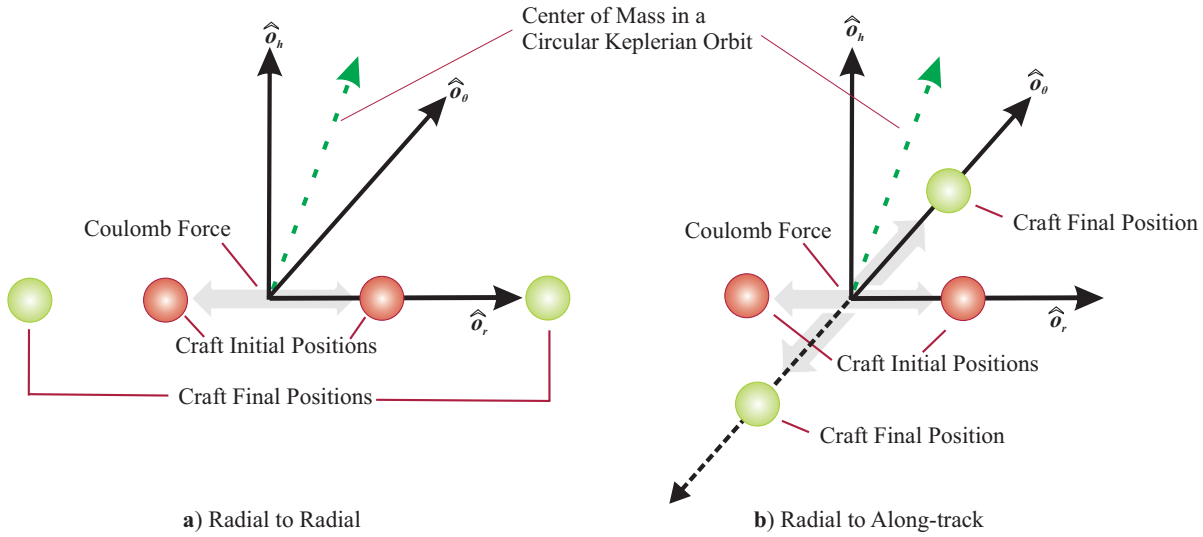

Figure 1: Two-Craft Reconfiguration Maneuvers

to choose proper minimum-fuel cost functions for correct problem formulation, and if a zero-cost (no fuel use needed) optimal trajectory is found, then it is the globally optimal solution. Using the pseudo-spectral method, a successful numerical implementation of an optimal control problem is demonstrated in Reference 15, where minimum-time reorientation of an asymmetric rigid body is considered. Therefore, prior work[11–15] motivates to explore the problems of repositioning or reorientation of Coulomb space structures using optimal control techniques.

Specifically, optimal reconfigurations of a two spacecraft Coulomb formation shown in Figure 1 are investigated in this paper using the calculus of variations approach with a Legendre pseudo-spectral method to numerically solve the optimal control problem. The objective is to use four performance measures to study optimal two-craft reconfigurations maximizing Coulomb propulsion usage for longitudinal maneuvers while utilizing minimum electric propulsion for transverse maneuvers. Therefore, the optimal reconfigurations of a two spacecraft formation using minimum-time, minimum-acceleration, minimum-fuel, and minimum-power performance measures are investigated by means of spectral methods. The paper is organized as follows. The basic optimal control problem for the general nonlinear system is discussed with given state-control constraints while minimizing a performance measure. Also, the necessary conditions for optimal control are presented which are derived from the application of Pontryagin's Minimum Principle, after which the nondimensionalized nonlinear equations of motion are derived for a two spacecraft Coulomb formation. Next, for two-craft reconfigurations, the optimal control problem formulation, various performance criteria, Pontryagin's necessary conditions, and the solution method are discussed. Finally, the open-loop numerical solutions of a two-craft formation in GEO circular orbits are presented and verified with Pontryagin's necessary conditions.

II. The Optimal Control Problem

The general family of optimal control problems considered in this paper can be stated as follows:[16–18] determine the state-control function pair, $\boldsymbol{x}(t), \boldsymbol{u}(t)$ over $[t_0, t_f]$ that minimize the cost functional,

$$J[\boldsymbol{x}(t), \boldsymbol{u}(t)] = E(\boldsymbol{x}(t_f), t_f) + \int_{t_o}^{t_f} F(\boldsymbol{x}(t), \boldsymbol{u}(t))dt \tag{1}$$

subject to

$$\text{equations of motion} \qquad \boldsymbol{f}(\boldsymbol{x}(t), \boldsymbol{u}(t)) - \dot{\boldsymbol{x}}(t) = 0 \tag{2}$$

$$\text{boundary constraints} \qquad b(\boldsymbol{x}(t_0), \boldsymbol{x}(t_f)) = 0 \tag{3}$$

where the functions E and F are called the *endpoint cost* and *running cost* respectively. The calculus of variations method can be used in solving the optimal control problem (OCP) subject to the conditions imposed at the initial and final time. Using this method, the cost functional takes a second form in terms of the adjoint variables. So, to conveniently formulate the problem and solve it as a two point boundary problem a control (or Pontryagin's) Hamiltonian is defined as

$$\mathcal{H}(\boldsymbol{x}(t), \boldsymbol{u}(t), \boldsymbol{\lambda}(t)) = F(\boldsymbol{x}(t), \boldsymbol{u}(t)) + \boldsymbol{\lambda}^T(t)\boldsymbol{f}(\boldsymbol{x}(t), \boldsymbol{u}(t)) \tag{4}$$

where $\boldsymbol{\lambda}(t)$ are the adjoint variables. The vanishing of the gradient of the Hamiltonian $\mathcal{H}$ provides the Pontryagin's necessary conditions for optimal control. Thus the state, adjoint and transversality necessary conditions for an optimal solution for all $t \in [t_0^*, t_f^*]$ are defined as:

$$\dot{\boldsymbol{x}}^*(t) = \frac{\partial \mathcal{H}}{\partial \boldsymbol{\lambda}}(\boldsymbol{x}^*(t), \boldsymbol{u}^*(t), \boldsymbol{\lambda}^*(t)) \tag{5}$$

$$\dot{\boldsymbol{\lambda}}^*(t) = -\frac{\partial \mathcal{H}}{\partial \boldsymbol{x}}(\boldsymbol{x}^*(t), \boldsymbol{u}^*(t), \boldsymbol{\lambda}^*(t)) \tag{6}$$

$$\left[\frac{\partial E}{\partial \boldsymbol{x}}(\boldsymbol{x}^*(t_f), t_f) - \boldsymbol{\lambda}^*(t_f)\right]^T \delta \boldsymbol{x}_f + \left[\mathcal{H}(\boldsymbol{x}^*(t_f), \boldsymbol{u}^*(t_f), \boldsymbol{\lambda}^*(t_f)) + \frac{\partial E}{\partial t}(\boldsymbol{x}^*(t_f), t_f)\right] \delta t_f = 0 \tag{7}$$

where $\boldsymbol{x}^*(t)$, $\boldsymbol{u}^*(t)$, and $\boldsymbol{\lambda}^*(t)$ is an optimal solution that satisfies the above necessary conditions.

III. Two-Craft Nonlinear Equations of Motion

The equations of motion for a two spacecraft Coulomb formation with hybrid thrusting (both electrostatic and inertial thrusting) are briefly derived in this section. The notation is similar to that used in Reference 10. In order to describe the relative motion of the satellite with respect to the formation center of mass a rotating Hill orbit frame $\mathcal{O} : \{\hat{\boldsymbol{o}}_r, \hat{\boldsymbol{o}}_\theta, \hat{\boldsymbol{o}}_h\}$ as shown in Figure 2 is chosen.[10] The formation center of mass is assumed to be the origin of this rotating Cartesian coordinate system and the relative position vector of the i^{th} satellite is defined as $\boldsymbol{\rho}_i = (x_i, y_i, z_i)^T$; where the x_i component is in the $\hat{\boldsymbol{o}}_r$ direction (orbit radial), the y_i is component in the $\hat{\boldsymbol{o}}_\theta$ direction of orbital velocity (along-track), and the component z_i is in the $\hat{\boldsymbol{o}}_h$ direction (orbit normal). The orbit frame origin coincides with the formation center of mass, and the center of mass position vector $\boldsymbol{r_c}$ is assumed to have a constant orbital rate of $\Omega = \sqrt{G\,M_e/r_c^3}$, where G is the gravity constant and M_e is the Earth's mass.

Assume that the two-craft formation is treated as a rigid body and aligned in the radial direction. For this orbit nadir aligned formation, consider a body fixed coordinate frame $\mathcal{B} : \{\hat{\boldsymbol{b}}_1, \hat{\boldsymbol{b}}_2, \hat{\boldsymbol{b}}_3\}$ where $\hat{\boldsymbol{b}}_1$ is aligned with the relative position vector $\boldsymbol{\rho_1}$ of mass m_1. In this configuration, the $\mathcal{O}$ and $\mathcal{B}$ frame orientation vectors are exactly aligned. Furthermore, the relative attitude between the $\mathcal{B}$ and $\mathcal{O}$ frames is represented using the 3-2-1 Euler angle notation ($\psi -$ pitch, $\theta -$ roll, $\phi -$ yaw). Using the direction cosine matrix expression given in Reference 10 to relate the $\mathcal{O}$ frame to $\mathcal{B}$ frame, the position vectors of mass m_1 and m_2 in the $\mathcal{O}$ frame are expressed as

$${}^{\mathcal{O}}\boldsymbol{\rho_1} = \begin{pmatrix} x_1 \\ y_1 \\ z_1 \end{pmatrix} = \frac{m_2 L}{m_1 + m_2} \begin{bmatrix} \cos\theta\,\cos\psi \\ \cos\theta\,\sin\psi \\ -\sin\theta \end{bmatrix} \tag{8a}$$

$${}^{\mathcal{O}}\boldsymbol{\rho_2} = \begin{pmatrix} x_2 \\ y_2 \\ z_2 \end{pmatrix} = \frac{m_1 L}{m_1 + m_2} \begin{bmatrix} -\cos\theta\,\cos\psi \\ -\cos\theta\,\sin\psi \\ \sin\theta \end{bmatrix} \tag{8b}$$

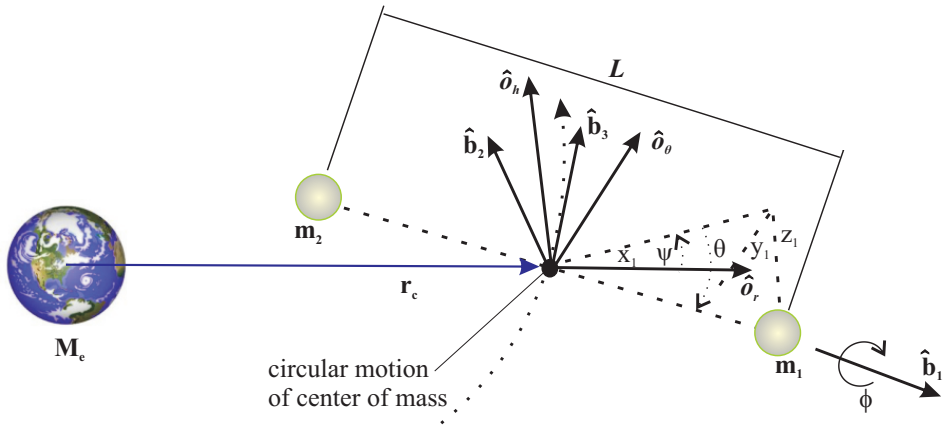

Figure 2: Euler Angles Representing the Attitude of Coulomb Tether with Respect to the Orbit Frame[10]

Furthermore, using the transport theorem,[19] the inertial velocity of mass m_i expressed in the $\mathcal{O}$ frame components becomes

$$^{\mathcal{O}}\boldsymbol{v_i} = \begin{pmatrix} \dot{x}_i - \Omega y_i \\ \dot{y}_i + \Omega\left(x_i + r_c\right) \\ \dot{z}_i \end{pmatrix} \tag{9}$$

Using Eqs. (8) and (9), the kinetic energy of the system is given by

$$T = \frac{1}{2}\frac{m_1 m_2}{m_1 + m_2}\left[\dot{L}^2 + L^2(\dot{\theta}^2 + (\dot{\psi} + \Omega)^2\cos^2\theta)\right] + \frac{1}{2}\left(m_1 + m_2\right)\Omega^2 r_c^2 \tag{10}$$

The gravitational potential energy retaining up to the second order terms is given by

$$V_g = -\frac{\mu}{r_c}(m_1 + m_2) + \frac{1}{2}\frac{\mu}{r_c^3}\frac{m_1 m_2}{m_1 + m_2}L^2(1 - 3\,\cos^2\theta\,\cos^2\psi) \tag{11}$$

and the associated Coulomb potential for the two-craft formation is[1]

$$V_c = k_c\frac{q_1 q_2}{L}\exp(-L/\lambda_d) \tag{12}$$

where q_i is the satellite charge and the parameter $k_c = 8.99 \times 10^9\ \mathrm{Nm^2/C^2}$ is Coulomb's constant. The exponential term in the expression depends on the Debye length parameter λ_d which controls the lower bound on the electrostatic field strength of plasma shielding between the craft. At Geostationary Orbits (GEO) the Debye length vary between 80-1400 m, with a mean of about 180 m.[20] The Coulomb spacecraft formation studied in this paper is assumed to be orbiting on high Earth orbits.

The nonlinear equations of motion are deduced from the Lagrangian $\mathcal{L} = T - (V_g + V_c)$ of the system in the following form

$$\begin{aligned} &\frac{\mathrm{d}}{\mathrm{d}t}\frac{\partial\mathcal{L}}{\partial\dot{q}^i} - \frac{\partial\mathcal{L}}{\partial q^i} = \mathcal{Q}_i \\ &q^i = (L, \psi, \theta) \quad (i = 1\ldots 3) \end{aligned} \tag{13}$$

where $\mathcal{Q}_i$ is the generalized force in the q^ith-degree of freedom excluding gravitational effects. For the circular orbit case, the nonlinear equations governing the separation distance L, the pitch angle ψ in the

orbital plane, and roll angle θ out-of-the orbital plane are

$$\ddot{L} - L(\dot{\theta}^2 + (\Omega + \dot{\psi})^2 \cos^2\theta - \Omega^2(1 - 3\cos^2\theta\, \cos^2\psi)) = \frac{\mathcal{Q}_L}{m} \tag{14a}$$

$$\ddot{\psi}\cos^2\theta - 2\dot{\theta}\sin\theta\, \cos\theta(\Omega + \dot{\psi}) + 2\frac{\dot{L}}{L}\cos^2\theta(\Omega + \dot{\psi}) + 3\Omega^2\, \cos^2\theta\, \cos\psi\, \sin\psi = \frac{\mathcal{Q}_\psi}{mL^2} \tag{14b}$$

$$\ddot{\theta} + 2\frac{\dot{L}}{L}\dot{\theta} + \cos\theta\, \sin\theta((\Omega + \dot{\psi})^2 + 3\Omega^2\, \cos^2\psi\,) = \frac{\mathcal{Q}_\theta}{mL^2} \tag{14c}$$

where $m = \frac{m_1 m_2}{m_1 + m_2}$, and $\mathcal{Q}_L$, $\mathcal{Q}_\psi$, $\mathcal{Q}_\theta$ are the generalized forces associated with L, ψ and θ, respectively. For a two spacecraft Coulomb formation, with F_{cf} being the Coulomb force acting between the two crafts, $\mathcal{Q}_L = -F_{\text{cf}}$, and is expressed as

$$F_{\text{cf}} = -k_c\frac{q_1 q_2}{L^2}\text{exp}(-L/\lambda_d)\Big(1 + \frac{L}{\lambda_d}\Big) \tag{15}$$

And $\mathcal{Q}_\psi = F_\psi L$ and $\mathcal{Q}_\theta = F_\theta L$ where F_ψ and F_θ are the electric propulsion (EP) thrusting forces that introduce net formation torques in the ψ and θ directions. Note that to avoid any potential plume exhaust impingement issues both the EP thruster forces are directed in orthogonal directions to the formation line of sight vector.

Further, to prevent numerical difficulties with very small numbers, Eqs. (14a) - (14c) are rescaled by defining the following nondimensional variables:

$$\tau = \Omega t, \qquad l = \frac{L}{L_{\text{ref}}}, \qquad u_l = \frac{F_{\text{cf}}}{m\Omega^2 L_{\text{ref}}}, \qquad u_\psi = \frac{F_\psi}{m\Omega^2 L_{\text{ref}}}, \qquad u_\theta = \frac{F_\theta}{m\Omega^2 L_{\text{ref}}} \tag{16}$$

where L_{ref} is the reference tether length. Therefore the radial equilibrium non-dimensional equations of motion become

$$l'' - l(\theta'^2 + (1 + \psi')^2\cos^2\theta - (1 - 3\cos^2\theta\, \cos^2\psi)) = -u_l \tag{17a}$$

$$\psi''\cos^2\theta + 2\cos\theta(\frac{l'}{l}\cos\theta - \theta'\sin\theta)(1 + \psi') + 3\cos^2\theta\, \cos\psi\, \sin\psi = \frac{u_\psi}{l} \tag{17b}$$

$$\theta'' + 2\frac{l'}{l}\theta' + \cos\theta\, \sin\theta((1 + \psi')^2 + 3\, \cos^2\psi\,) = \frac{u_\theta}{l} \tag{17c}$$

where the prime denotes the derivative with respect to non-dimensional time. And u_l, u_ψ and u_θ are the non-dimensional control variables. The control variable u_l is associated with Coulomb propulsion, and u_ψ and u_θ are related to electric propulsion. The equations of motion are coupled nonlinear ordinary differential equations.

Further, if the two-craft formation is treated as a rigid body and is aligned in one of the three equilibrium configurations (radial, along-track or orbitnormal directions), the ideal product of charges needed to achieve such static Coulomb formations are obtained from Eqs. (17) as

$$(q_1 q_2)_{\text{radial}} = -3\Omega^2\frac{L^3}{k_c}m\left(\frac{\lambda_d}{L + \lambda_d}\right)\text{exp}(L/\lambda_d) \tag{18a}$$

$$(q_1 q_2)_{\text{along-track}} = 0 \tag{18b}$$

$$(q_1 q_2)_{\text{orbitnormal}} = \Omega^2\frac{L^3}{k_c}m\left(\frac{\lambda_d}{L + \lambda_d}\right)\text{exp}(L/\lambda_d) \tag{18c}$$

Reference 10 obtained Eqs. (18) using the linearized dynamical models. Because the above constraints yield an infinite number of charge solutions, equal charges in magnitude across the craft are chosen. For

instance, for a radial equilibrium configuration assuming equal charges in magnitude and using Eqs. (15) and (18a) yields

$$q_1 = \sqrt{|(q_1 q_2)_{\text{radial}}|} \tag{19}$$

$$q_2 = -q_1 \tag{20}$$

IV. Reconfiguration Maneuvers

The formulation of any optimal control problem involves equations describing the dynamics of the system, the cost to be minimized, and any constraints which must be met to consider a solution valid. This section discusses the optimal control problem formulation for optimal two-craft formation reconfigurations, the four performance criteria used (minimum time, minimum acceleration, minimum propulsion fuel, and minimum power consumption), the Pontryagin's necessary conditions that any candidate optimal solution must satisfy, and the solution method of the optimal control problem.

A. Problem Statement

An optimum reconfiguration maneuver drives the two craft formation from its initial position given by $\boldsymbol{x}(\tau_0) = \boldsymbol{x}_0$ at nondimensional initial time τ_0 to its final position given by $\boldsymbol{x}(\tau_f) = \boldsymbol{x}_f$ at final time τ_f, while minimizing a cost function, subject to dynamical constraints. The state vector $\boldsymbol{x}$ is defined as

$$\boldsymbol{x} = (\psi, \psi^{'}, l, l^{'}, \theta, \theta^{'})^T \tag{21}$$

The four cost functions are defined below, and the dynamical constraints are presented in Eqs. (17). If $u_{\psi\text{max}}$ and $u_{\theta\text{max}}$ are the maximum thrust forces due to electric propulsion and $u_{l\text{max}}$ is the maximum thrust force due to Coulomb propulsion, then the control constraints are given by

$$-u_{\psi\text{max}} \leq u_\psi \leq u_{\psi\text{max}} \tag{22a}$$

$$-u_{l\text{max}} \leq u_l \leq u_{l\text{max}} \tag{22b}$$

$$-u_{\theta\text{max}} \leq u_\theta \leq u_{\theta\text{max}} \tag{22c}$$

If the unconstrained control appears non-linearly in either the state dynamics or the performance criterion (final time can be either fixed or free), the resulting optimal control solution results in continuous control. However, if the constrained control appears linearly, then the resulting optimal control solution results in bang-bang type controller.[16,17]

B. Measures of Optimality

Four measures of optimality are defined here that minimize a performance criterion (cost function) subject to dynamical constraints. The optimality criteria are minimum time, minimum acceleration of the separation distance between the two craft, minimum Coulomb and electric propulsion fuel consumption (modeled as the L^1-norm of the control acceleration) and minimum power consumption.

- *Minimum Time*

  Minimum time cost function belong to an important class of solutions for reconfiguration maneuvers. They set the lower bound on achievable time and the optimal control to obtain minimum-time response is maximum effort throughout the interval of operation.[17] The cost function to minimize is

  $$J = \int_{\tau_0}^{\tau_f} d\tau \tag{23}$$

  Generally time-optimal control solutions are of a bang-bang type.

- *Minimum Length Acceleration*

  For a 2-craft virtual Coulomb structure, it is desirable to keep the deployment/retrieval dynamics as smooth as possible for reconfigurations, so that the Coriolis forces balance the gravity gradient forces. Hence, minimizing the length acceleration is convenient performance measure to study. The cost function for a 2-craft Coulomb structure is

$$J = \int_{\tau_o}^{\tau_f} (l'')^2 d\tau \tag{24}$$

  which minimizes the total length acceleration, l'', appearing as a quadratic function.

- *Minimum Propulsion Fuel*

  This optimization criterion seeks to minimize the Coulomb and electric propulsion thrust magnitudes; the Coulomb thrust acts in the longitudinal direction and the electric propulsion thrusts are orthogonal to the formation line of sight vector in the ψ and θ directions of the rotating body frame. A thrust magnitude is directly related to the propulsion mass and the control acceleration. The minimum fuel cost function is expressed as

$$J = \int_{\tau_0}^{\tau_f} (W_{\text{cp}} |u_l| + W_{\text{ep}} |u_\psi| + W_{\text{ep}} |u_\theta|) d\tau \tag{25}$$

  where W_{cp} and W_{ep} are the weights associated with Coulomb propulsion and electric propulsion satisfying the condition $W_{\text{cp}} + W_{\text{ep}} = 1$. Since the cost associated with Coulomb propulsion is negligible compared to the electric propulsion (I_{sp} values of 10^8–10^{13} seconds versus 10^3–10^4 seconds), the weight associated with Coulomb propulsion is set to $W_{\text{cp}} = 0$, and accordingly $W_{\text{ep}} = 1$. However, for a radial equilibrium-to-equilibrium expansion or contraction reconfiguration there is no electric propulsion usage as such maneuvers require no inertial thrusting. Hence the minimum propulsion fuel cost function is not modeled for the radial-to-radial equilibrium reconfiguration cases. For other equilibrium-to-equilibrium reconfiguration maneuvers, the cost function becomes the fuel usage of the EP propulsion system:

$$J = \int_{\tau_0}^{\tau_f} (|u_\psi| + |u_\theta|) d\tau \tag{26}$$

  The cost function used here is the L^1 norm of the control instead of the quadratic cost function (L^2 norm squared), because L^1 measures fuel use and is thus the correct cost function for minimum fuel control. A quadratic cost-optimal controller takes more fuel.[14] Furthermore, quadratic cost controllers are continuous controllers which create new system engineering problems such as inducing undesirable effects on precision pointing payloads.[14] Therefore, the choice for the cost function formulation is the l^1 based L^1 norm ($\|\boldsymbol{u}(\tau)\|_{L^1} = \int \|\boldsymbol{u}(\tau)\|_{l^1} d\tau = \int (|u_1(\tau)| + \ldots + |u_n(\tau)|) d\tau$).

  Furthermore, the derivative of the l^1 based L^1 norm is discontinuous at zero, but the introduction of more control variables resolves this issue.[21] For example, in the ψ direction, the control vector is represented with two positive variables, a positive and negative measure of the control acceleration directed along the orthogonal directions to the formation line of sight vector. Both positive components have a lower bound of zero and an upper bound $u_{\psi\text{max}}$. As a consequence, the augmented control variables' derivatives are continuous and make the problem a smooth, nonlinear programming problem to solve. Also, only the negative or positive part of the control in one direction is nonzero at any given point in time.

- *Minimum Propulsion Power* The objective of this performance measure is to minimize total electric power required to engage the Coulomb and electric propulsion methods. The cost function is

$$J = \int_{\tau_0}^{\tau_f} (P_{\text{cp}}^2 + P_{\text{ep}}^2) d\tau \tag{27}$$

Assuming that the radii of the two-craft are the same, the Coulomb propulsion power P_{cp} required to maintain the spacecraft at some steady-state potential V_{sc} is[1]

$$P_{\text{cp}} = |V_{\text{sc}} I_{\text{e}}| \tag{28}$$

where the spacecraft potential V_{sc} and the current emitted I_{e} are given by

$$V_{\text{sc}} = \sqrt{\left| -k_c u_l m \Omega^2 \text{exp}(L/\lambda_d) \frac{L^2}{r_{\text{sc}}^2} \Big(\frac{\lambda_d}{L + \lambda_d} \Big) \right|} \tag{29}$$

$$I_{\text{e}} = 4\pi r_{\text{sc}}^2 J_{\text{p}} \tag{30}$$

where r_{sc} is the spacecraft radius in m, and J_{p} is the plasma current density in A/m^2. In the presence of the photoelectric effect, J_{p} as a function of the spacecraft potential is[1]

$$J_{\text{p}} = \begin{cases} J_{\text{e0}} \exp(\frac{-e|V_{\text{sc}}|}{kT_{\text{e}}}) - J_{\text{i0}} \left(1 + \frac{e|V_{\text{sc}}|}{kT_{\text{i}}}\right) - J_{\text{pe0}} & \text{for } V_{\text{sc}} < 0 \\ J_{\text{e0}} \left(1 + \frac{eV_{\text{sc}}}{kT_{\text{e}}}\right) - J_{\text{i0}} \exp(\frac{-eV_{\text{sc}}}{kT_{\text{i}}}) - J_{\text{pe0}} \exp(\frac{-eV_{\text{sc}}}{kT_{\text{pe}}})(1 + \frac{eV_{\text{sc}}}{kT_{\text{pe}}}) & \text{for } V_{\text{sc}} > 0 \end{cases} \tag{31}$$

with the electron, ion and photoelectron saturation currents given by $J_{\text{e0}} = en_{\text{e}}\sqrt{\frac{kT_{\text{e}}}{2\pi m_{\text{e}}}}$, $J_{\text{i0}} = -en_{\text{i}}\sqrt{\frac{kT_{\text{i}}}{2\pi m_{\text{i}}}}$ and J_{pe0}. The various plasma constants in Eq. (31) are the electron charge e in C, ion(electron) density $n_{\text{i(e)}}$ in m^{-3}, Boltzmann constant k in J/K, ion(electron) temperature $T_{\text{i(e)}}$ in K, T_{pe} is temperature of photoelectrons in K and the ion(electron) density $m_{\text{i(e)}}$ in kg. The experimental values of these plasma parameters during average GEO environment conditions are given in Reference 1.

The electric propulsion (EP) power P_{ep} is dependent on the control acceleration magnitude ($|u_\psi| + |u_\theta|$), thruster efficiency η, and specific impulse I_{sp}. Thus, P_{ep} is modeled as[22]

$$P_{\text{ep}} = m\Omega^2 L_{\text{ref}} \frac{(|u_\psi| + |u_\theta|) v_{\text{e}}}{2\eta} \tag{32}$$

where $v_{\text{e}} = gI_{\text{sp}}$ is the engine exhaust velocity. Xenon is assumed to be the propellant utilized for the EP system and the thruster efficiency η is determined by the relation

$$\eta = \frac{b v_{\text{e}}^2}{v_{\text{e}}^2 + d^2} \tag{33}$$

where $b = 0.81$ and $d = 13.5\text{km/s}$ are propellant-dependant coefficients derived from theoretical and experimental data.[22] For EP systems using xenon, the typical specific impulse limits are $1000\text{s} \leq I_{\text{sp}} \leq 7000\text{s}$.[22] I_{sp} is assumed to be constant over the entire maneuver which implies a fixed engine operating with no throttling. For this optimization criteria, the Coulomb and electric propulsion power levels are assumed to be of the same order (between 1 to 10 Watts).

C. Pontryagin's Necessary Conditions

Since the cost functions and the dynamical constraints do not explicitly depend on time, a necessary condition at an optimal solution where the cost functional is at a minimum is $\frac{\partial \mathcal{H}}{\partial t} = 0$. This condition along with the transversality condition in Eq. (7) provides the Hamiltonian function value at the optimal state-control function pair. At an optimal state-control function pair, for minimum time cost function the Hamiltonian function value is -1, and for minimum acceleration, minimum fuel, and minimum power cost functions the Hamiltonian function value is 0. These constant Hamiltonian function values for different performance criteria are later used to check the optimality of the numerical results.

D. Solution Method

Optimal control problems can rarely be solved analytically, and numerical methods are needed in such cases to solve them.[23] The first step is to discretize the problem, which is to define the system at discrete points which results in a finite number of variables because the system variables are only defined at the discrete points. The number of variables for the optimal control problem is then the number of variables in the system times the number of discretization points. The consequence of discretizing the optimal control problems explored here are nonlinearly unconstrained and constrained optimization problems. The unstable dynamics of the two-craft Coulomb formation require a more accurate representation of the maneuver to solve the problem. The optimal control problems in this paper are solved by the Legendre pseudo-spectral method.[18,24,25] Legendre pseudo-spectral method has the property that the solution will satisfy the necessary optimality conditions and eliminates traditional difficulties in solving for the costates in the optimal control problem.[26] Each optimal control problem in this paper is solved using the commercial software package DIDO. This powerful computational tool discretizes the problem by using the Legendre pseudo-spectral method and solves it using SNOPT, a sequential quadratic programming solver.[18] DIDO generates spectrally accurate solutions whose extremality can be verified using Pontryagin's Minimum Principle. Moreover, this tool can solve non-smooth problems that have state/control discontinuities where these discontinuities can be seen in bang-bang controls.

V. Numerical Study

This section presents numerical simulations illustrating ~~three~~ different optimal reconfigurations of a 2-craft Coulomb virtual tether formation in circular GEO orbits: radial spacecraft separation distance expansion and contraction maneuvers, radial to along-track maneuver with constant separation distance at the initial and final positions, and family of radial to along-track maneuvers. For each reconfiguration maneuver, four different performance criteria are considered for which optimal control solutions, associated state trajectories, and spacecraft charge time histories are presented. Eqs. (17) provide the equations of motion for these reconfiguration maneuvers. Table 1 provides the simulation parameters and their values. For each equilibrium-to-equilibrium reconfiguration, for bang-bang controls (minimum-time, minimum-fuel), the Coulomb propulsion thruster limit is fixed at a maximum equilibrium value of the maneuver. Therefore, the Coulomb thruster limit could vary depending on the maneuver under consideration, and from Eqs. (15) and (18), this limit is computed directly from the maximum equilibrium charge that can be produced. For example, for a radial-to-radial expansion, where the radial spacecraft separation distance is expanded from 25m to 35m, the charges vary from 1.45μC at 25m to 2.41μC at 35m which correspond to Coulomb forces of 29.91μN and 41.87μN respectively. Consequently, for this expansion, the Coulomb thruster limit is fixed at 41.87μN. For a similar expansion from 75m to 100m, the charges vary from 7.75μC to 12.21μC with Coulomb forces of 89.72μN and 119.62μN, and hence the limit is fixed at 119.62μN. For electric propulsion, a Colloid micro-thruster is used with a fixed limit of 30μN. Both the Coulomb and electric propulsion thruster limits can clearly go higher but such choices yield controls dominated by the respective thrusters. Furthermore, the perturbation forces due to the J_2 gravitational attraction and the solar radiation pressure at GEO are not considered in this simulation.

Table 1: Simulation Parameters Used for Reconfiguration Maneuvers

Parameter	Value	Units
m_1	150	kg
m_2	150	kg
L_{initial}	25	m
$u_{\psi\text{max}}$	30	μN
$u_{\theta\text{max}}$	30	μN
$I_{\text{sp}}(\text{EP})$	2000	sec
k_c	8.99×10^9	$\frac{\text{Nm}^2}{\text{C}^2}$
Ω	7.2915×10^{-5}	rad/sec

A. Radial Spacecraft Separation Distance Expansion and Contraction Maneuvers

This example illustrates how to optimally reconfigure a 2-craft Coulomb virtual tether formation to move the craft apart or closer using the Coulomb force and exploiting the gravity gradient to stabilize the formation. Numerical simulations are performed for two sets of maneuvers, expanding the radial Coulomb formation from an initial 25m to a final 35m and contracting the formation from a separation distance of 25m to 15m. The initial and final attitude values as well as the initial and final rates are set to zero through

$$\psi_i = \psi_f = \theta_i = \theta_f = \dot{\psi}_i = \dot{\psi}_f = \dot{\theta}_i = \dot{\theta}_f = \dot{L}_i = \dot{L}_f = 0 \tag{34}$$

For minimum-time, minimum-acceleration and minimum-power performance criteria, for an expansion maneuver in which the inter-craft distance increases from 25m to 35m, Figure 3 show the candidate in-plane trajectories, state histories, control solutions and the spacecraft charge time histories. The solutions are obtained for a choice of 100 nodes. Since the variations in the out-of-plane rotation angles (not shown) are negligible (on the order of 10^{-13} rad), only the in-plane trajectories are shown in Figure 3(a). The state histories in Figure 3(b) show that the boundary conditions are satisfied with viable variations of the in-plane rotation angles and the separation distances. The candidate control solutions in Figure 3(c) for minimum-time criteria display bang-bang characteristics, whereas, the minimum-acceleration and minimum-power criterion yields a continuous control solution. An end of a maneuver is denoted by a square box for the respective performance criterion. The charge on craft 2 will be equal and opposite to that of craft 1. Figure 3(d) shows the spacecraft charge time histories for one of the crafts. Since the magnitude of the control charges is on the order of micro-Coulombs, charge emission devices can be used in practice for implementation.

To verify that the control solution for each performance measure indeed drives the system from its known initial to the desired end state, the initial conditions and control solutions are used as input to the ode45 Matlab subroutine and the results are propagated. The propagated results (not shown) closely matched the pseudospectral approximations of the states, confirming the feasibility and convergence of the original solutions. Given the feasibility of the optimized solutions, the necessary conditions for optimality are examined. As previously stated, one such test is the approximate constancy of the Hamiltonian, whose theoretical constant value depends on the performance criterion. For the three performance measures, Table 2 shows that this necessary condition is indeed met. Table 2 also shows the optimal time required to complete the maneuver, maximum separation distance acceleration, and mean (root-mean-square - RMS) Coulomb propulsion thrust and power required. With the minimum-time criterion, the expansion is finished in 0.6584 orbits. Also, as an improvement over such a radial-expansion reconfiguration result of 1.8 days in Reference 10, which uses linearized time-varying dynamical models, the time taken using optimal control techniques is 0.65 days. Furthermore, optimal control techniques use variable separation distance rates as opposed to the

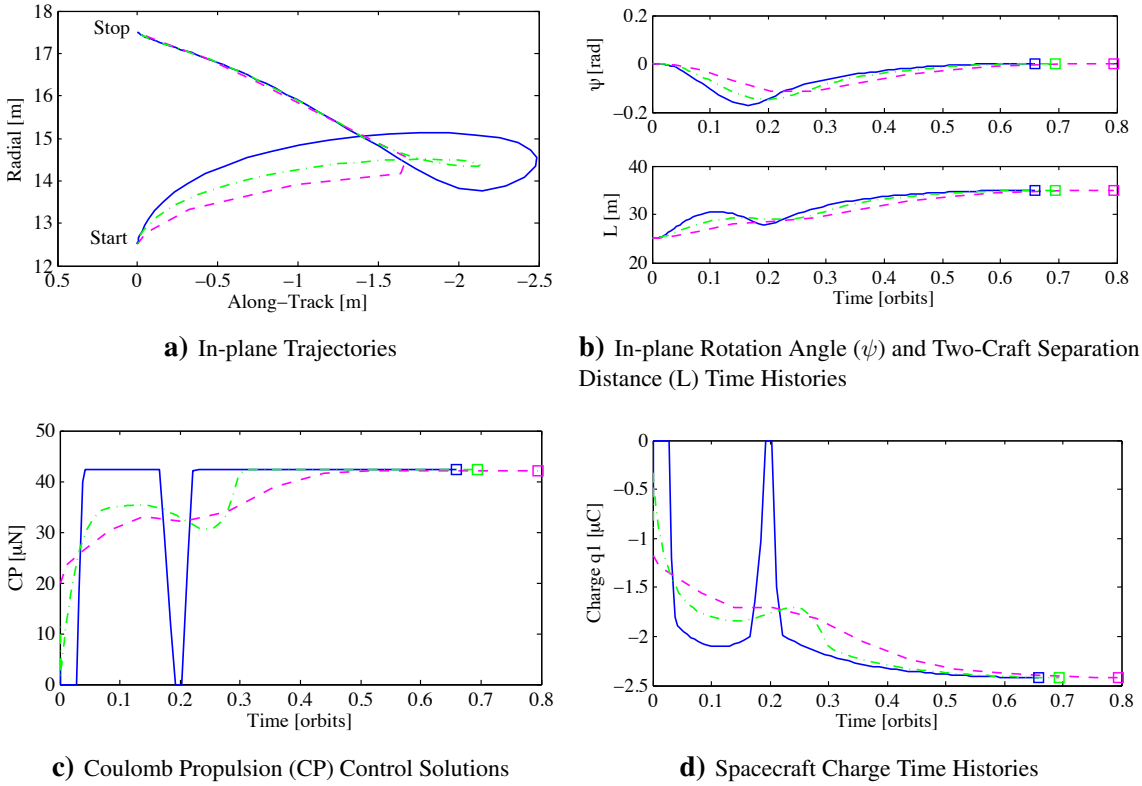

a) In-plane Trajectories

b) In-plane Rotation Angle (ψ) and Two-Craft Separation Distance (L) Time Histories

c) Coulomb Propulsion (CP) Control Solutions

d) Spacecraft Charge Time Histories

Figure 3: Simulation Results for Expanding the Radial Spacecraft Separation Distance from 25m to 35m. (— Min Time, – – Min Acceleration, – · – · Min Power)

constant rates used in Reference 10. The mean CP thrust and power required for the minimum-time criterion are high, and are low for the minimum-acceleration maneuver. For the minimum-acceleration criterion, the maximum Coulomb thrust needed at the end of the maneuver is 1μN greater than the radial equilibrium value of 41.8682μN at 35m. This discrepancy is necessary to overcome the formation's rotational dynamics, and at the end of the maneuver, the controls should explicitly drop down to the equilibrium value. Moreover, the maximum power requirements on the order of 10 Watts can be met by the Coulomb propulsion devices.

Table 2: Results for Expanding the Radial Spacecraft Separation Distance from 25m to 35m.

Cost	Time t_f orbits	Max L'' $\frac{\text{m}}{\text{s}^2}$	CP Thrust [RMS] μN	CP Power [RMS] W	Hamiltonian [Mean]
Min Time	0.6584	5.0053×10^{-7}	39.9401	10.1978	-1.0079
Min Acceleration	0.7958	0.1342×10^{-7}	38.4081	9.8661	-0.1983
Min Power	0.6934	3.7761×10^{-7}	38.3876	9.7835	0.0002

Figure 4 shows the state trajectories, state time histories, control solutions and the spacecraft charge time histories for a contraction maneuver in which the inter-craft distance decreases from 25m to 15m. The optimal solutions are symmetric to those of the expansion maneuver solutions. From the results of Table 3, the contraction maneuver for the minimum-time criterion finished in 0.7106 orbits. Also, as an improvement over such radial-contraction reconfiguration results from Reference 10 which take 1.8 days, the time taken using optimal control techniques is 0.71 days. However, the contraction took 1.27 days to complete for the

minimum-acceleration cost function. Similar to the expansion maneuver, the mean CP thrust and power required are highest for minimum-time criterion and are lowest for the minimum-acceleration criterion. For the minimum-time and minimum-power criteria, the maximum Coulomb thrust of 30.9027μN at the beginning of the maneuver is 1μN greater than the radial equilibrium value of 29.9059μN at 25m. This extra thrust is required at the beginning of the contraction to overcome the angular momentum which causes the in-plane motion to destabilize. At the end of the maneuver at 15m, the controls should explicitly drop down to the equilibrium value of 17.9435μN. Since the separation distances in the contraction maneuver are less than those of the expansion maneuver, the maximum power requirements are about 4 Watts.

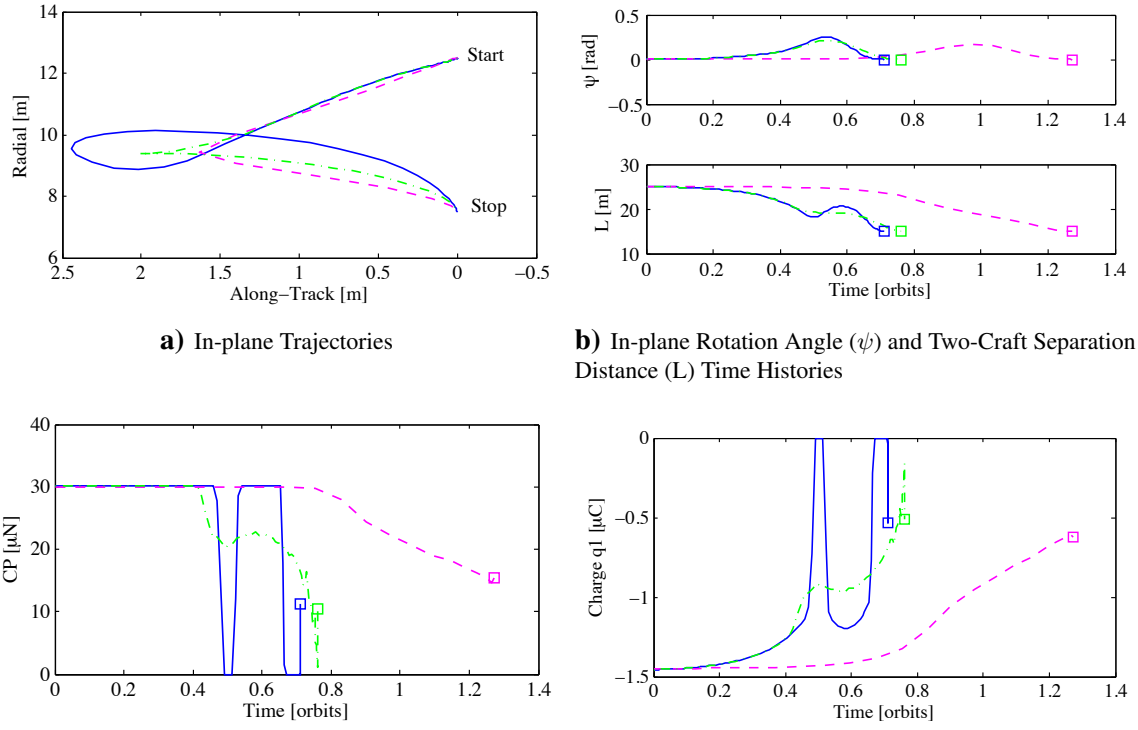

a) In-plane Trajectories

b) In-plane Rotation Angle (ψ) and Two-Craft Separation Distance (L) Time Histories

c) Coulomb Propulsion (CP) Control Solutions

d) Spacecraft Charge Time Histories

Figure 4: Simulation Results for Contracting the Radial Spacecraft Separation Distance from 25m to 15m. (— Min Time, – – Min Acceleration, – · – · Min Power)

Table 3: Results for Contracting the Radial Spacecraft Separation Distance from 25m to 15m.

Cost	Time t_f orbits	Max L'' $\frac{\text{m}}{\text{s}^2}$	CP Thrust [RMS] μN	CP Power [RMS] W	Hamiltonian [Mean]
Min Time	0.7106	3.4690×10^{-7}	27.8732	3.8127	-0.9951
Min Acceleration	1.2732	0.4384×10^{-7}	26.7043	3.8335	-0.0959
Min Power	0.7625	2.2591×10^{-7}	26.2355	3.5994	0.0001

B. Radial to Along-track Maneuver

The next example illustrates an optimal radial to along-track maneuver with the following boundary conditions

$$L_i = L_f = 25\,\text{m}, \psi_i = 0\,\text{rad}, \psi_f = -\pi/2\,\text{rad} \tag{35a}$$

$$\theta_i = \theta_f = \dot{\psi}_i = \dot{\psi}_f = \dot{\theta}_i = \dot{\theta}_f = \dot{L}_i = \dot{L}_f = 0 \tag{35b}$$

To utilize the rotational formation dynamics, the final in-plane attitude angle ψ_f is set to $-\pi/2\,\text{rad}$. Figure 5 shows the simulation results for a radial to along-track reconfiguration with a fixed separation distance of 25m at the initial and final equilibrium positions. The results for all four cost functions are obtained for a choice of 75 nodes. Figure 5(a) illustrates the in-plane trajectories for this maneuver. It is interesting to note that the minimum-fuel trajectory differs significantly from the others. The in-plane state histories in Figure 5(b) indicate that the boundary conditions are met. Figure 5(c) shows that the minimum-fuel maneuver uses maximum Coulomb thrusting, thus minimizing the EP thrusting usage. The charge histories in Figure 5(d) not only show the easily controllable charge magnitudes but also show the charge sign switching during the reconfiguration.

The propagated results (not shown) using ode45 closely matched the pseudospectral approximation of the states, thus verifying the feasibility and convergence of the solution. Moreover, as shown in Table 4, the constancy of the Hamiltonian value is satisfied for each performance measure. The final time required to complete the maneuver is a minimum of 0.22 days for the minimum-time criterion and is a maximum of 0.54 days for the minimum-acceleration criterion. The RMS power consumption shown in Table 4 indicates that more Coulomb propulsion is used over electric propulsion. For the maneuver, a maximum of about 4 Watts for Coulomb thrusting and a maximum of about 0.5 Watt for EP thrusting are utilized, easily meeting the power requirements of charge emission devices and Colloid thrusters. At the end of the maneuver at 25m at the along-track equilibrium position, the minimum-time, minimum-fuel and minimum-power controls should explicitly drop down to the equilibrium value of 0μN. The minimum-acceleration continuous control dropped down to the equilibrium value at the final time.

Table 4: Results of a Radial to Along-track Maneuver with 25m Separation Distance at the Initial and Final Positions.

Cost	Final Time t_f orbits	Max L'' $\frac{\text{m}}{\text{s}^2}$	CP Power [RMS] W	EP Power [RMS] W	Mean Hamiltonian
Min Time	0.2259	5.8934×10^{-7}	3.2953	0.5225	-0.9996
Min Acceleration	0.5440	6.0722×10^{-9}	2.1579	0.2246	-0.000013
Min Fuel	0.4419	2.5784×10^{-7}	1.5135	0.3772	0.0448
Min Power	0.3970	3.9874×10^{-7}	1.5770	0.2121	0.0005

Figure 6 shows the trajectories and controls for the same radial to along-track reconfiguration, but with the boundary conditions not utilizing the rotational formation dynamics. This implies that the final in-plane attitude angle ψ_f is set to $\pi/2\,\text{rad}$. The solutions are shown for all four cost functions and the in-plane trajectories are not very different to those of the solutions obtained utilizing the rotational formation dynamics. However, the control effort required for minimum-time exhibits sharp fluctuations which remained irrespective of the number of nodes chosen. Also, the reconfiguration times are longer compared to that of the reconfigurations with the boundary conditions utilizing the rotational formation dynamics. Furthermore, the simulation times between the two boundary conditions varied greatly, which are presented in detail in the next section.

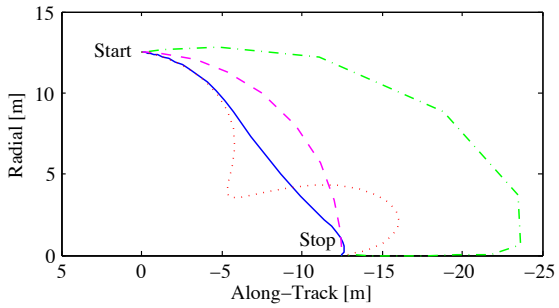

a) In-plane Trajectories

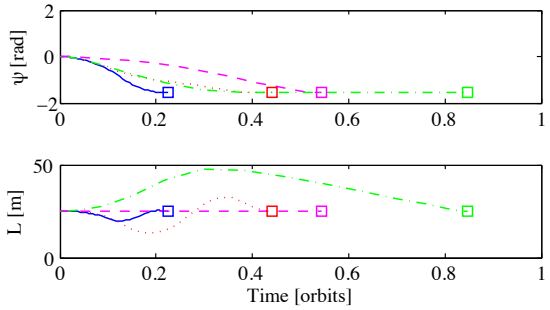

b) In-plane Rotation Angle (ψ) and Two-Craft Separation Distance (L) Time Histories

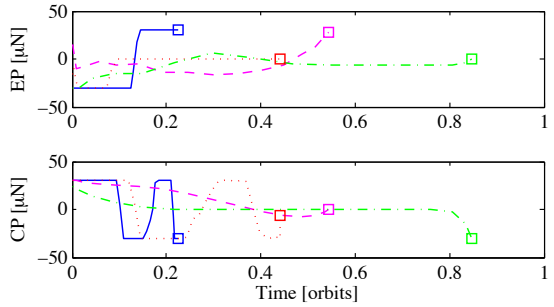

c) Electric Propulsion (EP) and Coulomb Propulsion (CP) Controls

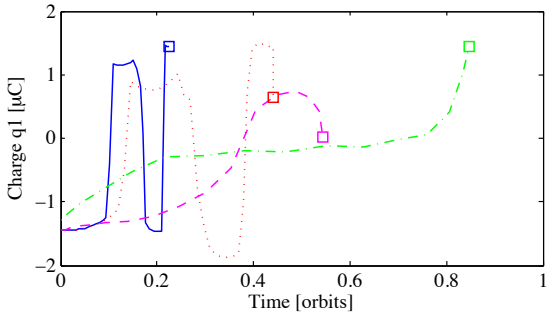

d) Spacecraft Charge Time Histories

Figure 5: Simulation Results of a Radial to Along-track Maneuver with 25m Separation Distance at the Initial and Final Positions. (— Min Time, – – Min Acceleration, · · · Min Fuel, – · – · Min Power)

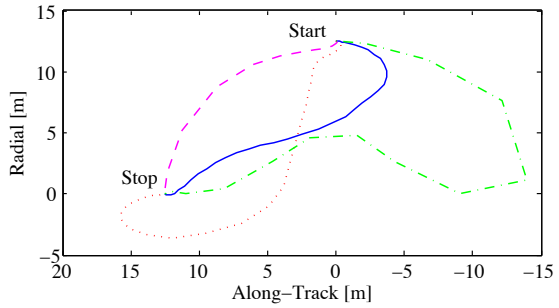

a) In-plane Trajectories

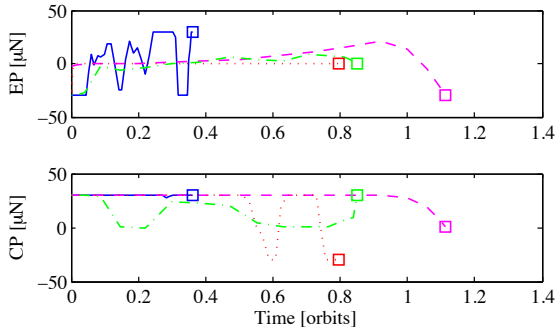

b) Electric Propulsion (EP) and Coulomb Propulsion (CP) Controls

Figure 6: Simulation Results of a Radial to Along-track Maneuver with 25m Separation Distance at the Initial and Final Positions with Boundary Conditions Not utilizing the Rotational Dynamics. (— Min Time, – – Min Acceleration, · · · Min Fuel, – · – · Min Power)

C. Family of Radial to Along-track Maneuvers

In this final example, a family of optimal maneuvers from radial to along-track equilibrium positions are illustrated. Figure 7 displays the Coulomb and electric propulsion controls (RMS) as a function of varying separation distances for each of the four cost functions. Each maneuver is performed with a fixed separation distance of 25m at the initial radial position, and varying final separation distances. Furthermore, the boundary conditions take advantage of the rotational formation dynamics of the two-craft system. The minimum-time performance measure consistently utilized more Coulomb and electric propulsion compared to the other measures. Whereas, for the minimum-power cost function, the Coulomb thrust used for two-craft separation distances between 90m and 125m is negligible (on the order of $10^{-5}\mu$N), and the EP thrust observed over the same distances is significantly higher. Another observation from Figures 7(a) and 7(b) is that minimum electric propulsion thrust is required for minimum-fuel cost function. The maneuver is able to use more Coulomb propulsion due to the exploitation of the rotational formation dynamics.

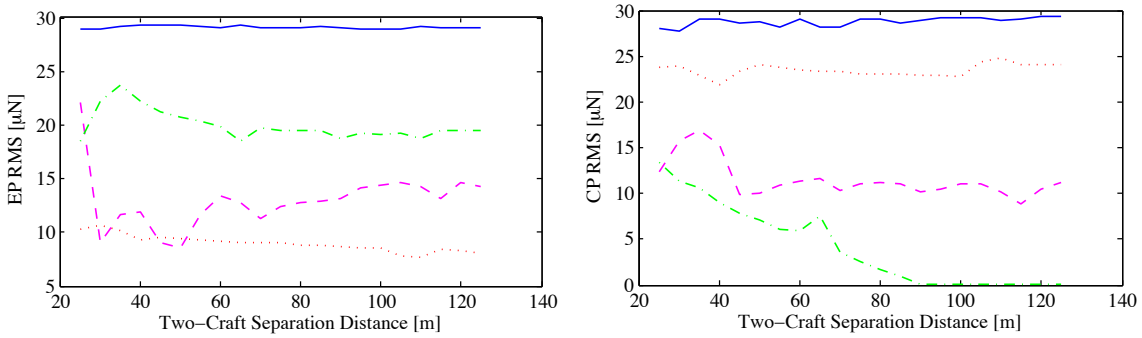

a) EP Controls **b)** CP Controls

Figure 7: In-plane Control Solutions for Family of Maneuvers from Radial to Along-track Equilibrium Position with Initial Separation Distance of 25m. (— Min Time, – – Min Acceleration, · · · Min Fuel, – · – · Min Power)

Figure 8 show results for two sets of maneuvers for the minimum-time performance measure. One set of maneuvers is generated with the boundary conditions taking advantage of the rotational formation dynamics (natural boundary conditions) and the other set is generated without taking advantage of the rotational formation dynamics (non-natural boundary conditions). Figure 8(a) shows the minimum-time trajectories with an initial separation distance of 25m between the craft and a final separation distance varying between 25m and 125m. Figure 8(a) also shows the closed-form natural solution using the Hill's equations[19] in which one craft is placed in the radial equilibrium position and allowed to drift in the absence of any Coulomb interaction with the second craft. Although the two sets of trajectories appear symmetric, collisions may occur with the other craft with non-natural boundary conditions. Also, the control solutions (not shown) exhibit sharp fluctuations for each maneuver with non-natural boundary conditions. Moreover, Figure 8(b) shows the numerical simulation times for each set of maneuvers which are much lower with the natural boundary conditions. For instance, in a worst-case scenario, with a separation distance of 125m, the simulation times for the non-natural boundary conditions are almost two orders of magnitude greater than those of obtained using the natural boundary conditions. Therefore, utilizing the natural formation dynamics yields clean bang-bang controls, collisionless trajectories and much lower simulation times.

VI. Conclusion

This paper presents an optimal-control framework for the reconfiguration of two-craft formations in circular orbits. Several in-plane reconfiguration problems are discussed, with each problem discretized using a Legendre pseudo-spectral method, and the resulting non-linear optimal control problems solved using the

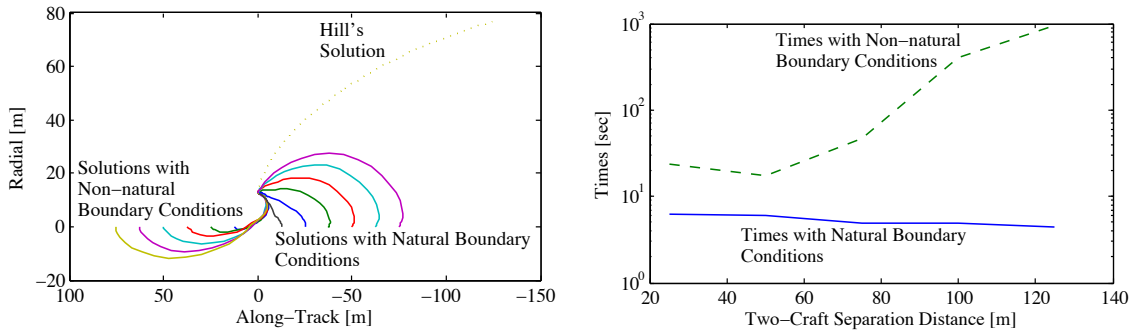

a) Spacecraft Trajectories **b)** Simulation Times

Figure 8: Minimum-Time Family of Maneuvers from Radial to Along-track Equilibrium Position with Initial Separation Distance of 25m.

software package DIDO. The feasibility and optimality of the open-loop numerical solutions are verified with Pontryagin's Minimum Principle. Four measures of optimality are discussed: minimum reconfiguration time, minimum acceleration of the separation distance, minimum power consumption, and minimum electric propulsion fuel usage. Results for these cost functions are illustrated for each reconfiguration problem with the goal of maximizing Coulomb propulsion usage while utilizing minimum electric propulsion. Because no linearizations are involved with nonlinear optimal control techniques, boundary conditions in the nonlinear regime hold. Previous Coulomb formation flying work used linearized time-varying dynamical models. Compared to previous work, the expansion and contraction reconfigurations in the radial direction are achieved in shorter times. Successful in-plane radial to along-track optimal reconfigurations for each performance measure are shown along with a family of minimum-time optimal maneuvers. For such maneuvers, the advantage of using natural formation dynamics in the selection of boundary conditions is highlighted. Not only are useful optimal reconfigurations for various problems found but interesting insights are given for respective cost functions. The optimal-control framework presented here can be extended to determine two-craft out-of-plane reconfigurations as well as to reconfigure three-craft formations.

References

[1]King, L. B., Parker, G. G., Deshmukh, S., and Chong, J.-H., "Spacecraft Formation-Flying using Inter-Vehicle Coulomb Forces," Tech. rep., NASA/NIAC, January 2002, http://www.niac.usra.edu.

[2]King, L. B., Parker, G. G., Deshmukh, S., and Chong, J.-H., "Study of Interspacecraft Coulomb Forces and Implications for Formation Flying," *AIAA Journal of Propulsion and Power*, Vol. 19, No. 3, May-June 2003, pp. 497-505.

[3]Berryman, J., and Schaub, H., "Analytical Charge Analysis for 2- and 3-Craft Coulomb Formations," *AIAA Journal of Guidance, Control and Dynamics*, Vol. 30, No. 6, Nov.-Dec. 2007, pp. 1701-1710.

[4]Vasavada, H., and Schaub, H., "Analytic Solutions for Equal Mass 4-Craft Static Coulomb Formation," *Journal of Astronautical Sciences*, Vol. 56, No. 1, January-March 2008, pp. 7-40.

[5]Berryman, J., and Schaub, H. "Static Equilibrium Configurations in GEO Coulomb Spacecraft Formations," *AAS/AIAA Space Flight Mechanics Meeting*, Copper Mountain, CO, Jan. 23-27, 2005. Paper No. 05-104.

[6]Parker, G. G., Passerello, C. E., and Schaub, H., "Static Formation Control using Interspacecraft Coulomb Forces," *2nd International Symposium on Formation Flying Missions and Technologies*, Washington D.C., Sept. 14-16, 2004.

[7]Parker, G. G., King, L. B., and Schaub, H., "Steered Spacecraft Deployment Using Interspacecraft Coulomb Forces," *American Control Conference*, Minneapolis, Minnesota, June 14-16 2006. Paper No. WeC10.5.

[8]Pettazzi, L., Krger, H., Theil, S., and Izzo, D., "Electrostatic Forces for Satellite Swarm Navigation and Reconfiguration," *Technical Report*, ESA, Doc.No.: ARI-SS-FP-ZAR-001, 2006.

[9]Pettazzi, L., and Izzo, D., "Self-Assembly of Large Structures in Space Using Intersatellite Coulomb Forces," *56th International Astronautical Congress*, Fukuoka, Japan, Oct.17-21 2005. Paper IAC-06-C3.4/D3.4.07.

[10]Natarajan, A., "A Study of Dynamics and Stability of Two-Craft Coulomb Tether Formations," *Ph.D. Dissertation*, Aerospace and Ocean Engineering Department, Virginia Polytechnic Institute and State University, Blacksburg, VA, May 2007.

[11]Steindl, A., and Troger, H., "Optimal control of deployment of a tethered subsatellite," *Nonlinear dynamics* Vol. 31, No. 3, 2003, pp. 257-274.

[12]Steindl, A., Steiner, W., and Troger, H., "Optimal control of retrieval of a tethered subsatellite," *Solid Mech. Appl.* 122, 2005, pp. 441-450.

[13]Williams, P., and Trivailo., "On the optimal deployment and retrieval of tethered satellites," *The 41st AIAA/ASME/SAE/ASEE Joint Propulsion Conference and Exhibit* Tucson, 10-13 July 2005.

[14]Ross, I. M., "How to Find Minimum-Fuel Controllers," *Proceedings of AIAA Guidance, Navigation, and Control Conference*, AIAA 2004-5346, Providence, Rhode Island, Aug. 16-19, 2004.

[15]Fleming, A., Sekhavat, P., and Ross, I. M., "Minimum-Time Reorientation of an Asymmetric Rigid Body," *AIAA Guidance, Navigation and Control Conference and Exhibit*, AIAA-2008-7012, Honolulu, Hawaii, 2008.

[16]Bryson, D.E., *Dynamic Optimization*, Addison-Wesley Longman, Inc., 1999.

[17]Kirk, D.E., *Optimal Control Theory: An Introduction*, Prentice-Hall, Inc., Englewood Cliffs, NJ, 1970.

[18]Ross, I. M., "A Beginners Guide to DIDO: A MATLAB Application Package for Solving Optimal Control Problems," *Elissar Technical Report TR-711*, http://www.elissar.biz, 2007.

[19]Schaub, H., and Junkins, J. L., "Analytical Mechanics of Space Systems," *AIAA Education Series*, Reston , VA , 2003.

[20]Romanelli, C. C., Natarajan, A., Schaub, H., Parker, G. G., and King, L. B., "Coulomb Spacecraft Voltage Study Due to Differential Orbital Perturbations," *AAS/AIAA Space Flight Mechanics Meeting*, Tampa Florida, January 22-26, 2006. Paper No. AAS 06-123.

[21]Ross, I. M., "Space Trajectory Optimization and L^1-Optimal Control Problems," *Modern Astrodynamics*, pp. 155-188, Elsevier Astrodynamics Series, 2006.

[22]Kluever, C. A., "Heliospheric Boundary Exploration Using Ion Propulsion Spacecraft," *Journal of Spacecraft and Rockets*, Vol. 34, No. 3, May-June 1997, pp. 365-371.

[23]Betts, J. T., "Survey of Numerical Methods for Trajectory Optimization," *Journal of Guidance, Control, and Dynamics*, Vol. 21, No. 2, 1998, pp. 193-207.

[24]Ross, I. M., "A Roadmap for Optimal Control: The Right Way to Commute," *Annals of the New York Academy of Sciences*, Vol. 1065, pp. 210-231, 2006.

[25]Ross, I. M., Sekhavat, P., Fleming, A., and Gong, Q., "Optimal feedback control: foundations, examples, and experimental results for a new approach," *Journal of Guidance, Control, and Dynamics*, Vol. 31, No. 2, 2008, pp. 307-321.

[26]Fahroo, F., and Ross, I. M., "Costate Estimation by a Legendre Pseudospectral Method," *Proceedings of AIAA Guidance, Navigation, and Control Conference*, AIAA-98-4222, Monterey, CA 93943, 1998.